Supplementary Information for

Improved Synthesis of $Ti_3C_2T_x$ MXene Resulting in Exceptional Electrical Conductivity, High Synthesis Yield, and Enhanced Capacitance

Ali Shayesteh Zeraati[1,2], Seyedalireza Mirkhani[1], Pengcheng Sun[2], Michael Naguib[3], Paul V. Braun[2,], Uttandaraman Sundararaj[1,*]*

[1]*Department of Chemical and Petroleum Engineering, University of Calgary, 2500 University Dr NW, Calgary, Canada T2N 1N4*
[2]*Department of Materials Science and Engineering, Materials Research Laboratory, Beckman Institute for Advanced Science and Technology, University of Illinois at Urbana–Champaign, Urbana, IL 61801 United States*
[3]*Department of Physics and Engineering Physics, Tulane University, New Orleans, Louisiana 70118, United States*
*Corresponding Authors' Emails: pbraun@illinois.edu and u.sundararaj@ucalgary.ca

Experimental Section/Methods

$Ti_3C_2T_x$ MXene synthesis: In this study, $Ti_3C_2T_x$ MXene was prepared by two different approaches: (i) MILD[1, 2] and EN-MILD (Evaporated-Nitrogen MILD) methods. In both approaches, a 125 ml polyethylene container with an outer diameter of about 40 mm and height of about 90 mm was used as the etching container. The place of N_2 inlet and outlet is shown in **Figure S1**. For the MILD approach, LiF (1.6 g; ≥ 99.98% trace metals basis, Sigma-Aldrich, USA) was added to 9 M HCl (20 ml; made using ACS reagent 37 wt%, Sigma-Aldrich, USA) and continuously stirred for 30 minutes at 40 °C. After completely dissolving LiF in HCl solution, Ti_3AlC_2 (1 g; Carbon-Ukraine, Particle size <40 µm and used as received) was added in course of 30 minutes and the reaction was run for 24 h. Then, the etching product was washed thoroughly as will be explained later.

In EN-MILD approach, the reaction vessel was purged by dry nitrogen throughout the etching reaction.

This would lead to the partial evaporation of the etching solution, which gradually increases the acids and salt concentrations over time. 1.6 g of LiF was added to 20 ml of 9 M HCl solution and stirred for 30 minutes at 40 °C under nitrogen (same concentration and condition as MILD approach). Then, Ti_3AlC_2 MAX phase (1 g) was added to the etching solution in course of 30 minutes and the mixture was stirred at 300 rpm for the duration of etching reaction. EN-MILD approach reaction was run for different etching time of 6 h, 12 h, 18 h, 24 h, and 30 h. These time intervals were selected to investigate the effect of the N_2 purging on the synthesized MXene. The nitrogen flow rate (for this volume of etchant and the container's dimension) in EN-MILD approach was about 250 SCCM. This flow rate should be optimized (based on the final volume of etchant) if another reaction container or a different volume of etchant is being used. All the synthesis was conducted in a designed HF fume hood and handling chemicals should be done carefully following strict safety protocols for handling HF containing solutions. The outlet of the etching container was introduced into a condenser before being vented directly into fume hood.

As shown in **Figure S1**, the final volume of the etching solution is critical and affecting the concentration of HF and Li-ions in the etching solution. Using etching containers with different volume/dimension with the same N_2 pressure results in different volumes for final etching solution. Industrial grade of Praxair nitrogen with a purity level of 99.998% was used for the MXene synthesis. After completion of etching reaction (MILD and EN-MILD), the etched material was copiously washed with Millipore water *via* centrifugation. In each washing step, the acidic mixture was divided into four 50 ml centrifuge tubes, diluted with Millipore to almost 50 ml, and centrifuged at 3500 rpm (1917 rcf) for 5 minutes. After each cycle, the acidic supernatant was decanted, and the sediment was dispersed in almost 50 ml fresh Millipore water. It is worth noting that washing the etched product with about 800 ml of Millipore water was required to reach pH of about 6 (**Figure S1**). After discarding the supernatant, the sediment was diluted using 20-30 ml Millipore water and sonicated in an ice-bath (with a temperature less than 4 °C) under dry N_2 atmosphere for 10 minutes. It is worth mentioning that 10 min bath sonication was replaced with hand shaking (that has been used with others) to ensure reproducibility. The suspension was centrifuged for an hour @ 3500 rpm (1917 rcf) to separate the single layer (few layer) MXene flakes from un-etched MAX phase or thick multi-layer MXene sheets. The homogeneous delaminated $Ti_3C_2T_x$ supernatant was stored in a fridge @ 4 ºC to use for sample preparation. The concentration of the MXene colloidal suspensions was calculated by vacuum filtration of a known suspension volume through a polypropylene membrane (kindly provided by Celgard, pore size 0.064 μm) and measuring the weight of the prepared film after 4 h drying at 60 °C under vacuum. The synthesis yield is defined as the amount of MXene in this supernatant (which is mostly single layer flake; after washing the etched material, 10 min sonication and centrifugation for 1 h) to the initial amount of MAX phase. Typically, we obtained ~ 60% synthesis yield of single layer MXene by sonication (10 min) and 30-40 % by handshaking (10 min) when EN-MILD approach was used with 24 h etching time. The values reported in this manuscript were obtained with 10 min sonication. Some samples were collected before the final stage of

sonication/centrifugation to study the etching efficiency by XRD and SEM (results are shown in **Figure 1** and **Figure S2**). Freestanding MXene papers were prepared by vacuum filtration with a Celgard membrane (pore size 0.064 μm) and the films' thickness was tailored by controlling the concentration and volume of the initial MXene solution.

*Materials' characterization***:** The scanning electron microscopy (SEM) images of MXene flakes on alumina membrane were taken using a Hitachi S-4800 (Tokyo, Japan) SEM operated at 5 kV. To do this, a drop of dilute colloidal solution of different MXenes was placed on porous alumina substrate (Anodisc, 0.1 μm pore size, Whatman) and then dried under vacuum. SEM imaging on MAX/MXene powder and the cross-sections of freestanding MXene film in addition to the thickness measurement of these freestanding films were performed by using a Thermo Scios2 Dual-Beam SEM/Focused Ion Beam (FIB). Because of the importance of freestanding film thickness on electrical conductivity values, the SEM/FIB thickness measurements were used in calculations. High-resolution transmission electron microscopy (HRTEM) images were captured with a Scanning/Transmission electron microscope (STEM/TEM) at 80 kV (FEI Themis Z-TEM, Thermo Fisher Scientific Company). The microscope was equipped with energy dispersive X-ray spectroscopy (EDS) system for chemical analysis. STEM samples were prepared by dropping of the dilute colloidal solution of different MXenes on the carbon side of a standard TEM copper grid covered with holey carbon film, and then placed on a filter paper to quickly dry. All atomic force microscopy (AFM) images were captured with an Asylum Research AFM operated in tapping mode in air. For this purpose, the dilute colloidal solution of different MXenes was drop-casted onto freshly cleaved mica (Ted Pella Inc). The elemental composition and chemical structure of different freestanding MXene films were investigated by X-ray photon spectroscopy (XPS) using a Kratos Axis Ultra equipped with monochromatic Al X-ray source. Binding energies were referenced to the C1s peak of (C-C, 284.8 eV) bond and the peak fitting was carried out using CasaXPS Version 2.3.19 RP 1.0 in a similar manner as Ref.[3] X-ray diffraction (XRD) spectra were recorded using PANALYTICAL

PHILLIPS X'PERT MRD (used for freestanding films) and SIEMENS/BRUKER D-5000 (used for powder samples) systems with Cu K-alpha radiation source with a counting time of 1.0°/min at 40 kV and 44 mA. PerkinElmer (Nexion 350D) inductively coupled plasma (ICP-MS) was used to determine the concentration of titanium and lithium in the MXene free-standing papers. The ^{1}H, ^{7}Li and ^{19}F NMR experiments were carried out using a Bruker Avance III HD equipped with a 500-MHz, 5-mm, BBFO CryoProbe. These characterizations were performed to measure the ions concentrations in the etchant solution after 24 h at 40 °C under MILD approach condition and with dried nitrogen purging. The sheet resistances of MXene freestanding films were measured by four-point probe measurements (Jandel 4-Point probe). Each electrical conductivity value was calculated by an average of 10 different measurements.

Electrochemical measurements: All electrochemical tests were conducted by three-electrode plastic Swagelok cells using a VMP3 potentiostat/galvanostat (Biologic). In the cell, a large extra activated carbon (Alfa Aesar) film was used as the counter electrode, MXene sheet supported by a glassy carbon current collector was the working electrode and Ag/AgCl (in 1 M KCl) was the reference electrode. Aqueous 3 M H_2SO_4 electrolyte and a glass fibre filter as the separators were used in the tests. All the electrodes were pre-cycled for 20 cycles using Cyclic Voltammetry (CV) at 20 mV s^{-1} before the actual electrochemical tests were performed. The CV tests for different MXene electrodes were performed at scan rates of 1-1000 mV s^{-1}. Galvanostatic charge-discharge (GCD) cycling was performed at current densities from 1 to 20 A g^{-1}. Galvanostatic cycling was performed at 20 A g^{-1} to study the cyclability of the prepared electrodes over 10,000 cycles. The specific capacitance of the MXene electrodes was calculated using the GCD curve based on the following formula:

$$C_s = \frac{I \times \Delta t}{m \times \Delta V}$$

where C_s (F g^{-1}) is the gravimetric specific capacitance; I (mA) is the discharge current; Δt (s) is the discharge time from the charge-discharge curve; ΔV (V) is the potential window; and m (mg) is the electrode mass. Volumetric capacitances for different MXene electrodes were calculated using the volume of the electrode (instead of mass) in the equation.

Table S1 shows the details of dataset presented in **Figure 1a**, the electrical conductivity of MXene synthesized with direct HF approach and *in-situ* HF approaches (clay, modified clay, original MILD, and modified MILD).

Table S1. The details of data presented in Figure 1a

Sample	Synthesis approach (-/ 1.0g MAX)	Synthesis time & Temperature	Conductivity (S cm^{-1})	Ref.
$Ti_3C_2T_x$	0.66 g LiF + 10 ml 6.0M HCl	24 h at 40°C	6500	4
$Ti_3C_2T_x$	0.66g of LiF + 10 ml 6M HCl	45 h at 40 °C	1500	5
$Ti_3C_2T_x$	1.0 g LiF + 20 ml 6.0M HCl	24 h at 35°C	4800	1
$Ti_3C_2T_x$	1.0 g LiF + 20 ml 6.0M HCl	24 h at 35°C	2200	6
$Ti_3C_2T_x$	1.0 g LiF + 20 ml 6.0M HCl	24 h at 35°C	6760	7
$Ti_3C_2T_x$	1.0 g of LiF + 20 ml 6M HCl	24 h at 35 °C	4600	8
$Ti_3C_2T_x$	1.98 g LiF + 30 ml 6.0M HCl (1.2 MAX)	45 h at 40°C	1250	9
$Ti_3C_2T_x$	1.0 g LiF + 10 ml 9.0M HCl	24 h at 35°C	1215	10
$Ti_3C_2T_x$	1.0 g LiF + 10 ml 9.0M HCl	24 h at 35°C	4556	11
$Ti_3C_2T_x$	1.0 g LiF + 10 ml 9.0M HCl	24 h at 35 °C	32.5	12
$Ti_3C_2T_x$	1.0 g LiF + 25 ml 9.0M HCl	24 h at 45°C	1500	13
$Ti_3C_2T_x$	1.0 g LiF + 20 ml 9.0M HCl	24 h at 35°C	9880	14
$Ti_3C_2T_x$	1.0 g LiF + 20 ml 9.0M HCl	72 h at 50°C	1000	15
$Ti_3C_2T_x$	1.0 g LiF + 20 ml 9.0M HCl	24 h at 35°C	5000	16
$Ti_3C_2T_x$	1.0 g LiF + 20 ml 9.0M HCl	24 h at 35°C	4000	17
$Ti_3C_2T_x$	1.6g of LiF + 20 ml 9M HCl	40 h at RT	4400	18
$Ti_3C_2T_x$	1.6 g LiF + 20 ml 9.0M HCl	24 h at RT	8000	2
$Ti_3C_2T_x$	1.6 g LiF + 20 ml 9.0M HCl	30 h at 50 °C	15100	19
$Ti_3C_2T_x$	1.6 g LiF + 20 ml 9.0M HCl	30 h at 50 °C	13200	19
$Ti_3C_2T_x$	1.6 g LiF + 20 ml 9.0M HCl	30 h at 50 °C	10500	19

Sample	Synthesis approach (-/ 1.0g MAX)	Synthesis time & Temperature	Conductivity (S/cm)	Ref.
$Ti_3C_2T_x$	1.6 g LiF + 20 ml 9.0M HCl +Proton acid treatment	36 h at RT	10400	[20]
$Ti_3C_2T_x$	10 mL of HCl + LiF solution	24 h at 40 °C	1836	[21]
$Ti_3C_2T_x$	10 ml of 40%wt HF	18 h at RT	2650	[22]
$Ti_3C_2T_x$	10 ml of 50.0 wt% HF	18 h at RT	2402.4	[23]
$Ti_3C_2T_x$	30 ml of 40%wt HF	24 h at RT	2230	[24]
$Ti_3C_2T_x$	2 ml HF + 12 ml HCl + 6 ml DI water, LiCl	24 h at RT	~8500	[25]
$Ti_3C_2T_x$	2 ml HF + 12 ml HCl + 6 ml DI water, LiCl	24 h at RT	~8500	[25]
$Ti_3C_2T_x$	3 ml 49 wt% HF + 6 ml 12 M HCl + 1 ml DI water, LiCl	24 h at RT	~14000	[26]
$Ti_3C_2T_x$	Calcination MXene film@800°C	Calcination @ 1hr	2410	[27]
$Ti_3C_2T_x$	Electrodeposition	-	7400	[28]
V_2CT_x	20ml HF +TMAOH	48 h at 35 °C	~ 1000	[25]
$Nb_yV_{2-y}CT_x$	20ml HF +TMAOH	48 h at 35 °C	~ 19-349	[25]
Nb_2CT_x	20ml HF +TMAOH	48 h at 35 °C	~ 5	[25]
$Mo_2TiC_2T_x$	20ml HF +TMAOH	48 h at 50 °C	~ 49	[25]
$Nb_4C_3T_x$	20ml HF +TMAOH	168 h at 50 °C	~ 75	[25]
$Mo_2Ti_2C_3T_x$	20ml HF +TMAOH	96 h at 50 °C	~ 227	[25]
Ti_2C	10% HF	10h	0.147	[29]
Ti_2C	4 g LiF + 40 ml 11.7M HCl	24 h at 35 °C	5250	[30]
Mo_2C	14M HF, TBAOH	160h at 35 °C	4.35	[31]
Mo_2N	Ammoniation of Mo_2C	600 °C	2083	[32]
V_2N	Ammoniation of Mo_2C	600 °C	4166	[32]
Ti_3CN	0.66g LiF + 10ml 6.0M HCl	12 h at 30 °C	1045	[33]
Mo_2TiC_2	10ml HF 48%+TBAOH	48 h at 55 °C	50	[34]

Sample	Synthesis approach (-/ 1.0g MAX)	Synthesis time & Temperature	Conductivity (S/cm)	Ref.
$Mo_2Ti_2C_3$	10ml HF 48%+TBAOH	90 h at 55 °C	100	34
$Mo_2TiC_2T_x$	10 ml of 10.0 wt% HF + 10 wt% HCl	40 h at 40°C	100	1
$Mo_2Ti_2C_3T_x$	10 ml of 10.0 wt% HF + 10 wt% HCl	40 h at 40°C	250	1
V_2C	10 ml 12 M HF	72 h at 50 °C	3250	35
Mo_2C	40 ml of 25 wt% HF, TBAOH	160 h at 55 °C	0.8	36
V_2C	14 M HF, TBAOH	24 h at 35 °C	384.6	37
Nb_2CT_x	50 wt% HF	90 h at 35 °C	0.0164	38
TiNbC	50 wt% HF	28 h	0.192	39
Ti_3CN	30 wt% HF	18 h	0.27	39
Nb_4C_3	50 wt% HF	96 h	2.17	39
Ta_4C_3	50 wt% HF	72 h	0.476	39
Ti_3CNT_x	2 ml HF + 12 ml HCl + 6 ml DI water, LiCl	24 h at RT	~2700	25
Ti_2CT_x	2 ml HF + 12 ml HCl + 6 ml DI water, LiCl	24 h at RT	~1600	25

Figure S1-a illustrates the EN-MILD synthesis procedure. In the MILD approach, HF is formed by reaction of LiF and HCl. In our approach, purging dry nitrogen in the synthesis stage was used to minimize the dissolved oxygen in water and evaporate the etching solution to increase the HF concentration. The volume (**Figure S1-b**) of the etching solutions were measured for the MILD approach (after 24 h) and for EN-MILD approach after 6 h, 12 h, 18 h, 24 h, and 30 h. This volume changes can be used as an indication for the pressure of nitrogen flow. **Figure S1-c** shows the ions concentration of the etching solution prepared with MILD approach and EN-MILD approach after 24 h. The measurement shows that the acid and Li ion concentrations increased with the EN-MILD approach. **Figure S1** also

illustrates that Li ion concentration increases which can improve the intercalation/exfoliation procedure. pH changes during washing stage; pH≈ 6 was achieved after 4 cycles of washing (**Figure S1-d**).

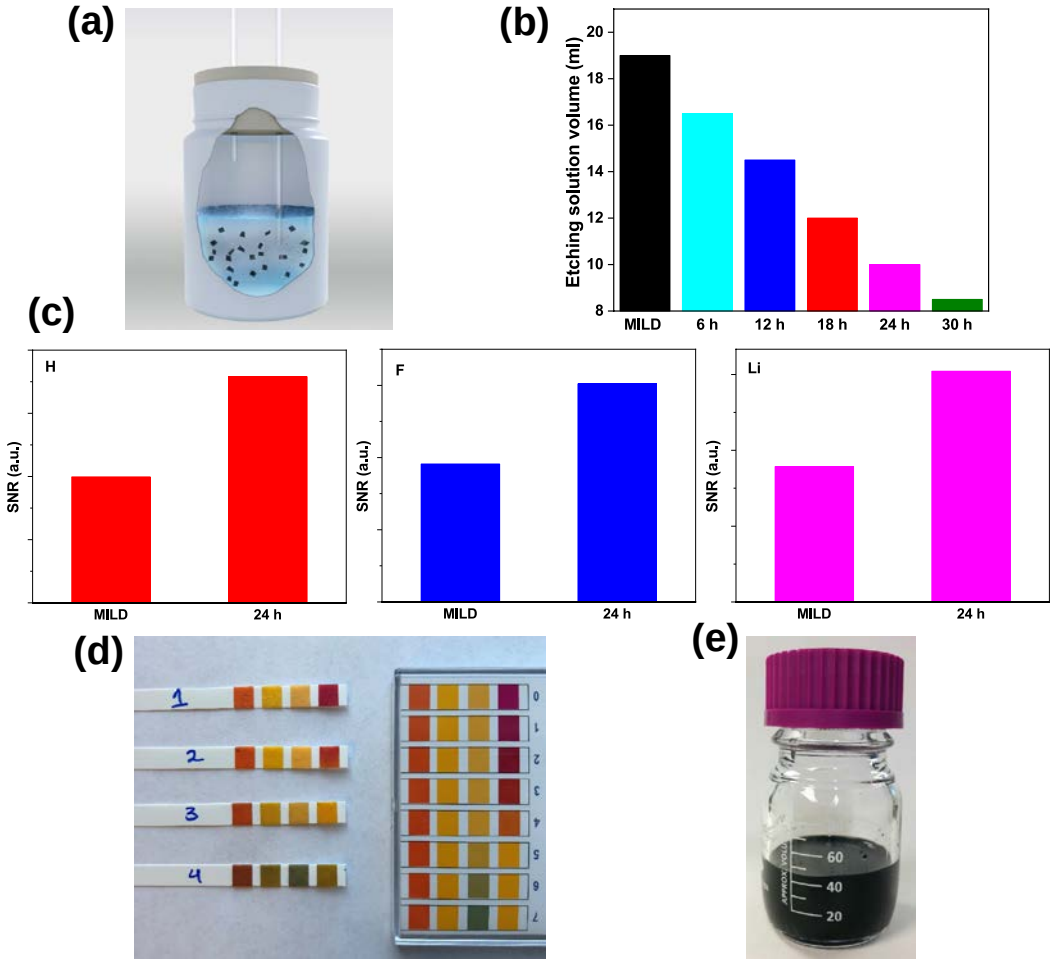

Figure S1. (a) Synthesis vial connected to the nitrogen source and a vent. This help to minimize the oxygen in the etchant and make concentrated etching solution; (b) Comparison of volume of etching solution in MILD method and our method for different etching times; (c) H, F, and Li ions concentration in etching solution prepared with MILD approach and EN-MILD approach after 24 h; (d) pH variations after the centrifuge cycles (1, 2, 3, and 4) during washing; (e) Optical images of stable aqueous solutions of $Ti_3C_2T_x$ prepared at 24 h with the EN-MILD approach. The concentration of the colloidal MXene can be easily reached to 31 mg/ml.

The amount of HF which is formed through the reaction between HCl and LIF can be estimated using the below reaction. We calculate estimated concentration of HF in reaction of 1.6 g LiF with 20 ml of 9M HCl as follows:

$$LiF\ (s) + HCl\ (aq) \rightarrow LiCl\ (aq) + HF\ (aq)$$

Table S2. The estimated concentration of HF according to the reaction between HCl and LiF

Material	Molecular Weight	Initial conc. (mol)	Final conc. after reaction (mol)	Final mass (g)	wt% (Water included)
HF	20	0	0.06	1.20	4.90
HCl	36.46	0.18	0.12	4.37	17.85
LiF	25.93	0.06	0	0	0
LiCl	42.39	0	0.06	2.54	10.37

For water/HCl solution, we suppose that $\Delta V_{mixing} = 0$ and stock solution of hydrochloric acid is 12.18 M based on a density of 1.2 g/mL, a molecular weight of 36.46 g/mol, and a concentration of 37% w/w. We also assume that LiF is completely consumed during the reaction. To prepare 20 ml of 9 M HCl, 14.78 ml of HCl (37 wt%) should be mixed with 5.22 ml of water. So:

$$m_{water} = 14.781 \times 1.2 \times 0.63 + 5.2 = 16.37\ g$$

We assumed that the yield of reaction is 100%, in other words, all LiF is consumed during reaction. However, it may not be the case in the reaction and the above values are the upper limit. In another word, less HF is produced compared to the above calculated values. Gradual increase of acid concentrations (HCl and HF) and consumption of HF through the reaction (MAX phase etching) results in dissolving more LiF. To further examine the effect of gradually increasing the acids and LiF concentrations through the etching (EN-MILD approach) on electrical conductivity, we performed an experiment with a higher HCl concentration and more LiF to possibility create a higher concentration of

HF. **Table S3** summarizes the electrical conductivity of $Ti_3C_2T_x$ MXene synthesized at different conditions.

Table S3. The electrical conductivity of $Ti_3C_2T_x$ MXene synthesized at different conditions

Sample	Synthesis approach (-/ 1.0g MAX)	Synthesis time (h)	Conductivity (S cm^{-1})	Ref.
$Ti_3C_2T_x$	1.0 g LiF + 20 ml 6.0M HCl	24 h at 35°C	4800	[1]
$Ti_3C_2T_x$	1.6 g LiF + 20 ml 9.0M HCl	24 h at RT	8000	[2]
$Ti_3C_2T_x$	1.0 g LiF + 20 ml 6.0M HCl	48 h at 35°C	3700	**This work**
$Ti_3C_2T_x$	1.6 g LiF + 20 ml 9.0M HCl	24 h at 40°C	5800	
$Ti_3C_2T_x$	2 g LiF + 20 ml 12.2M HCl	24 h at 40°C	900	
$Ti_3C_2T_x$	1.6 g LiF + 20 ml 9.0M HCl (EN-MILD)	24 h at 40°C	2.4×10^4	

The results demonstrate the advantages of using EN-MILD approach on achieving higher electrical conductivity compared to using higher concentrations of acid from the beginning of etching stage or longer etching time. Etching MAX phase starts with the smaller particles due to their higher surface area (higher reactivity) and then proceeds to larger MAX particles. By employing a higher acid concentration from the beginning, the chance of defect formation, oxidation, and over-etching increases for smaller particles as the etched small particles will remain in contact with the highly concentrated acid the entire time of the treatment. This will lead to lower electrical conductivity. However, by gradually increasing the acids concentration, exposure of smaller MAX particles to high acid concentration will be less, compared to the case where the etching reaction starts with high etchant concentration. This decreases the chance for defect formation and excessive oxidation. EN-MILD approach is also useful for etching the larger unreacted MAX particles when higher acid concentrations are available at later stages of etching.

Figure S2 shows the XRD patterns for the MAX phase and MAX/MXene powders obtained by MILD and the EN-MILD approach after 6 h and 12 h etching. These MAX/MXene powders were collected after last cycle of washing and dried in vacuum oven for 4 h at 60 °C. The main peak of MAX phase about 2θ ≈ 39º was almost removed even after 6 h etching indicating the efficiency of the EN-MILD approach on removing the Al layer. As clearly shown, after etching the MAX phase with HCl and LiF, (0002) peak shifted to lower angles which confirms higher *d*-spacing. This can be attributed to the substitution of H_3O^+ with Li ions that swell the interlayer space and eventual exfoliation.[40]

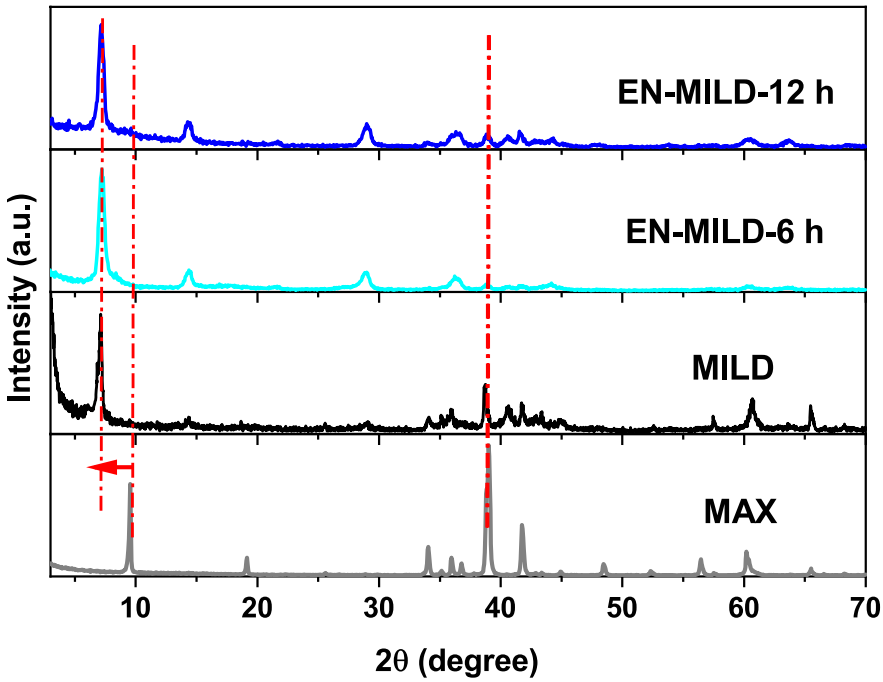

Figure S2. XRD patterns of Ti_3AlC_2 MAX powder and MAX/MXene powders prepared with MILD approach and EN-MILD approach after 6 h and 12 h etching. The main MAX peak at 2θ ≈ 39º almost diminished for the modified approach, demonstrating the efficiency of proposed etching approach. The (0002) peak of MAX at 2θ ≈ 9.6º was shifted to lower degrees indicating the opening of the structure caused by etching.

Table S4. *d*-spacing for (0002) peaks for different MXene synthesized in this work

Etching time	**(0002) peak degree**	**Interlayer spacing** (A^{o})
MILD	7.40	11.94
EN-MILD 12 h	7.42	11.90
EN-MILD 18 h	7.38	11.97
EN-MILD 24 h	7.17	12.34
EN-MILD 30 h	7.14	12.37

Table S5. Synthesis (delamination) yield of single layer MXene and colloidal concentration for $Ti_3C_2T_x$ MXene reported in the literature and in this study

MXene	Synthesis approach (-/ 1.0g MAX)	Synthesis time and temperature	Colloidal conc. (mg/ml)	Delamination yield (%)	Ref.
$Ti_3C_2T_x$	1.0 g LiF + 10 ml 9.0M HCl	24 h at 35°C	3.6	18%	[41]*
$Ti_3C_2T_x$	1.6 g LiF + 20 ml 9.0M HCl	24 h at RT	1.0-2.0	-	[2]
$Ti_3C_2T_x$	1.0 g LiF + 20 ml 6.0M HCl	24 h at 35°C	10.0	-	[42]§
$Ti_3C_2T_x$	1.0 g LiF + 20 ml 9.0M HCl	26 h at 35°C	1.0	-	[43]
$Ti_3C_2T_x$	1.0 g LiF + 10 ml 9.0M HCl + 0.3 g of $AlCl_3 \cdot 6H_2O$	72 h at RT	2.01	-	[44]•
$Ti_3C_2T_x$	1.0 g LiF + 20 ml 9.0M HCl	24 h at 35°C	0.5	-	[45]
$Ti_3C_2T_x$	Electrochemical etching	5 h at RT	-	40	[46]
$Ti_3C_2T_x$	10 ml HF 50% + Hydrothermal -assisted intercalation	24 h at 60°C for etching + 24 h at 140°C for intercalation	1.5	74	[47]∫
$Ti_3C_2T_x$	Etching and Microwave-assisted	-	-	10-20	[48]
$Ti_3C_2T_x$	25 % aqueous tetramethylammonium hydroxide (TMAOH)	-	1.05	-	[49]
$Ti_3C_2T_x$	**1.6 g LiF + 20 ml 9.0M HCl**	**24 h at 40°C (EN-MILD)**	**31.6**	**60%**	**This work**

*2.0 g of MAX phase was used for the synthesis in addition to 1 h sonication which may lead to a higher colloidal concentration.

§ 2.0 g of MAX phase was used for the synthesis in addition to 30 min tip sonication which may lead to a higher colloidal concentration.

• The etched powder was dispersed on 10 mL of TMAOH (25 wt % in water) for 72 h.

∫ Ti_3AlC_2 was firstly etched with HF and then etched material was hydrothermally intercalated. The synthesis yield was defined based on the amount of intercalated MXene to the etched MXene powder in the intercalation procedure. The low electrical conductivity of 405 S/cm was reported for this high synthesis yield.

Figure S3 displays the size distribution obtained by AFM measurement. As can be seen, EN-MILD 24 h MXene has the largest flake size. 200 individual MXene flakes were used for the statistical analysis.

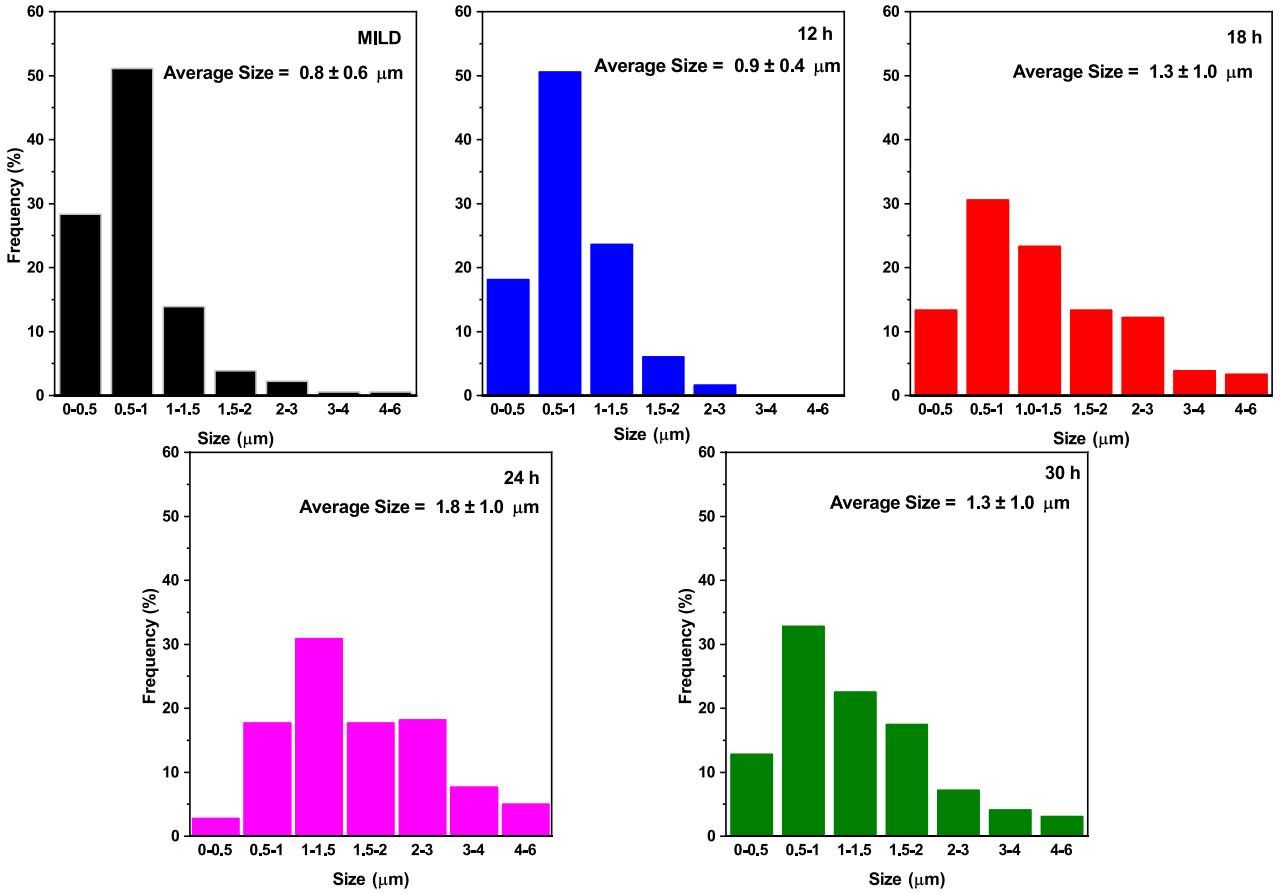

Figure S3. Size distribution analysis from AFM of MXene samples at different synthesis conditions: MILD, 12 h, 18 h, 24 h, and 30 h. The analysis shows that MXene synthesized at 24 h using EN-MILD approach leads to the largest flakes size.

Figure S4 demonstrates the synthesis yield and MXene flake size follow the same trends in EN-MILD approach.

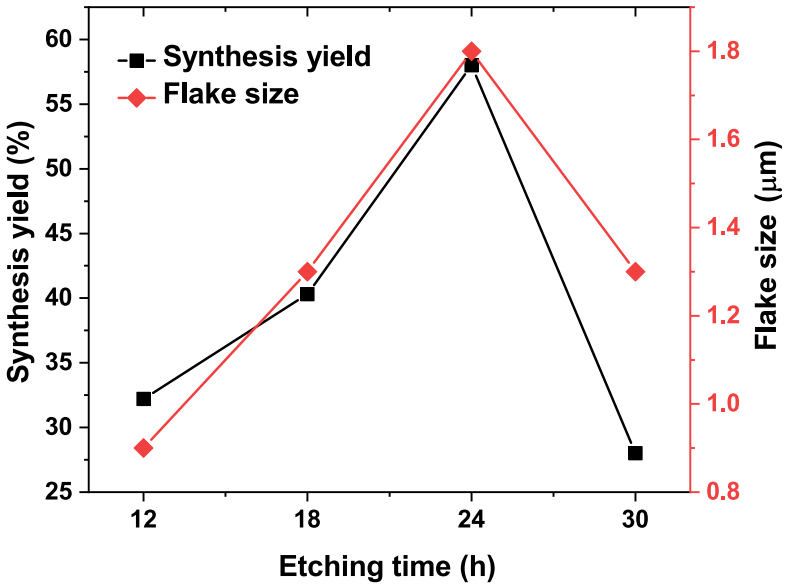

Figure S4. Synthesis yield and flake size at different etching time using EN-MILD approach.

Figure S5 illustrates MXene flakes prepared with MILD and EN-MILD approaches at 24 h etching time.

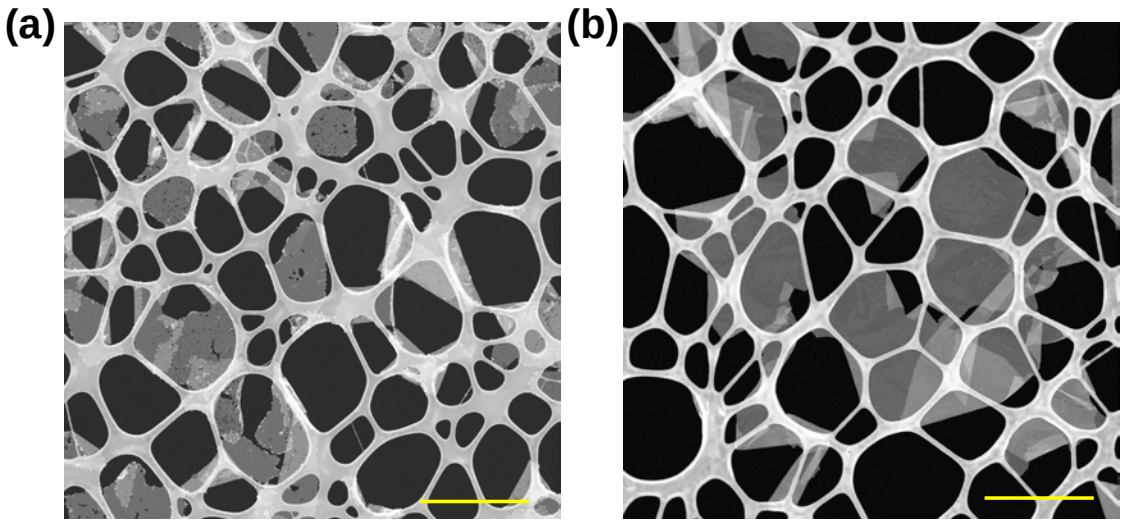

Figure S5. a and b represent dark-field STEM images of MILD and EN-MILD samples at the same etching time, 24 h, respectively. Scale bar is 1.0 μm.

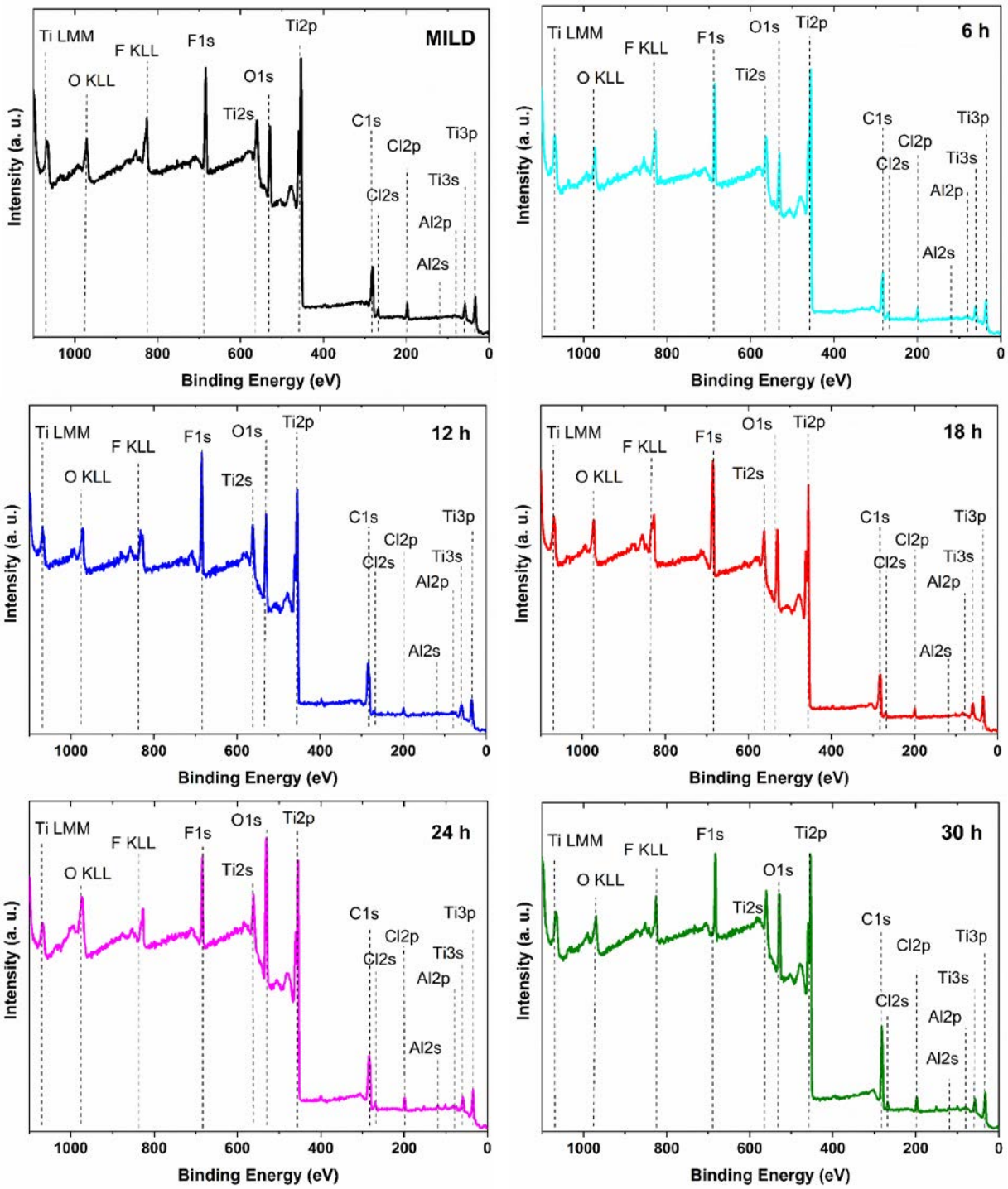

Figure S6. XPS survey of the prepared MXene with MILD and EN-MILD approach after different etching time intervals; 6 h, 12 h, 18 h, 24 h, and 30 h and their elemental analysis.

The elemental analysis demonstrates that the amount of oxygen is increasing while the amount of Ti is decreasing in EN-MILD etching. Preparing MXene at higher etching time can lead to higher oxygen functional groups.

Table S6. Atomic percentages obtained from XPS analysis

Element (at%) / Samples	Ti	C	O	F	Al	Cl	(F+Cl):Ti
MILD	26.2 ± 0.3	41.2 ± 0.4	18.6± 0.2	10.3± 0.1	0.5± 0.1	3.2± 0.2	0.52
6 h	31.4 ± 0.4	40.4 ± 0.2	13.7± 0.3	11.1± 0.2	1.2± 0.3	2.2± 0.3	0.42
12 h	28.3 ± 0.3	41.2 ± 0.4	18.2± 0.2	9.8± 0.3	0.7± 0.1	1.8± 0.1	0.41
18 h	26.4 ± 0.2	41.9 ± 0.3	21.0± 0.3	8.9± 0.2	0.4± 0.05	1.4± 0.2	0.39
24 h	23.1 ± 0.1	43.1 ± 0.6	24.9± 0.1	7.5± 0.4	0.2± 0.1	1.2± 0.1	0.38
30 h	22.5 ± 0.4	51.8 ± 0.5	16.7± 0.3	5.9± 0.7	0	3.1± 0.5	0.40

Tables S7-S9 demonstrate the details of fitting for high-resolution peaks for Ti2p, C1s, and O1s. The fitting shows that using EN-MILD approach in longer etching time (24 h) led to more oxygen functional groups that can be beneficial for charge storage applications.

Table S7. Details of peak fitting for high resolution of Ti2p

Sample	*BE (eV)*	*FWHM (eV)*	*Fraction (%)*	*Assigned to*	*References*
$Ti_3C_2T_x$-12h	454.64 (458.92)	1.08 (1.58)	21.54	(OH, or O)-Ti-C	[3, 50-54]
	455.28 (460.79)	1.14 (1.66)	27.74	(OH, or O)-Ti(II)	
	456.12 (461.91)	1.62 (1.66)	35.11	(OH, or O)-Ti(III)	
	457.37 (462.83)	1.43 (1.29)	10.71	TiO_2	
	458.30 (463.74)	1.16 (1.66)	4.9	Ti-F	
$Ti_3C_2T_x$-18h	454.75 (459.1)	1.07 (1.66)	21.4	(OH, or O)-Ti-C	[3, 50-54]
	455.38 (460.96)	1.11 (1.66)	29.21	(OH, or O)-Ti(II)	
	456.22 (462.01)	1.57 (1.66)	33.9	(OH, or O)-Ti(III)	
	457.37 (462.83)	1.29 (1.36)	10.3	TiO_2	
	458.23 (463.74)	1.16 (1.51)	5.2	Ti-F	
$Ti_3C_2T_x$-24h	454.77 (459.1)	1.06 (1.66)	22.58	(OH, or O)-Ti-C	[3, 50-54]
	455.37 (460.91)	1.13 (1.56)	28.76	(OH, or O)-Ti(II)	
	456.20 (461.92)	1.57 (1.66)	35.68	(OH, or O)-Ti(III)	
	457.37 (462.83)	1.27 (1.13)	8.38	TiO_2	
	458.29 (463.61)	1.16 (1.16)	4.6	Ti-F	
$Ti_3C_2T_x$-MILD	454.73 (459.1)	1.08 (1.66)	21	(OH, or O)-Ti-C	[3, 50-54]
	455.33 (460.91)	1.14 (1.66)	32.3	(OH, or O)-Ti(II)	
	456.11 (461.92)	1.62 (1.47)	31.32	(OH, or O)-Ti(III)	
	457.29 (462.83)	1.17 (1.08)	12.81	TiO_2	
	458.37 (463.61)	0.66 (1.66)	3.56	Ti-F	
$Ti_3C_2T_x$-30h	454.66 (459.1)	1.01 (1.66)	17.73	(OH, or O)-Ti-C	[3, 50-54]
	455.28 (460.91)	1.17 (1.66)	38.63	(OH, or O)-Ti(II)	
	456.19 (461.92)	1.48 (1.49)	28.47	(OH, or O)-Ti(III)	
	457.29 (462.83)	1.75 (0.99)	12.34	TiO_2	
	458.39 (463.61)	0.66 (1.66)	2.84	Ti-F	

Table S8. Details of peak fitting for high resolution of C1s

Sample	*BE (eV)*	*FWHM (eV)*	*Fraction (%)*	*Assigned to*	*References*
$Ti_3C_2T_x$-12h	281.41	0.87	37.53	C-Ti-T_x	3, 50, 54-56
	284.59	1.93	51.48	C-C	
	286.24	0.93	4.6	C-O	
	286.98	1.1	1.92	HO-C=O	
	288.92	1.69	4.48	C-F	
$Ti_3C_2T_x$-18h	281.57	0.86	42.63	C-Ti-T_x	3, 50, 54-56
	284.67	1.93	45.04	C-C	
	286.28	1.07	4.18	C-O	
	287.11	1.32	2.99	HO-C=O	
	289.26	1.93	5.15	C-F	
C-$Ti_3C_2T_x$-24h	281.5	0.93	38.21	C-Ti-T_x	3, 50, 54-56
	284.69	1.71	43.24	C-C	
	286.09	0.93	4.88	C-O	
	286.66	0.93	3.23	HO-C=O	
	288.26	1.93	10.44	C-F	
$Ti_3C_2T_x$-MILD	281.64	0.91	40.04	Ti-C	3, 50, 54-56
	284.55	2.62	49.68	C-C	
	286.26	0.88	2.46	C-O	
	288.53	1.21	2.36	HO-C=O	
	289.76	1.28	5.47	C-F	
$Ti_3C_2T_x$-30h	281.99	0.86	30.44	C-Ti-T_x	3, 50, 54-56
	284.68	2.1	62.88	C-C	
	286.64	1.22	4.43	C-O	
	288.54	2.22	1.26	HO-C=O	
	289.09	1.22	0.98	C-F	

Table S9. Details of peak fitting for high resolution of O1s

Sample	*BE (eV)*	*FWHM (eV)*	*Fraction (%)*	*Assigned to*	*References*
$Ti_3C_2T_x$-12h	529.91	1.08	33.22	C-Ti-O(I)$_x$	3, 50-52
	531	1.68	32.96	C-Ti-O(II)$_x$	
	532.16	1.25	11.36	C-Ti-(OH)$_x$	
	533.08	1.26	9.1	Al_2O_3/OR‡	
	533.8	2.18	13.37	H_2O_{ads}	
$Ti_3C_2T_x$-18h	529.95	1.05	35.32	C-Ti-O(I)$_x$	3, 50-52
	531	1.68	29.17	C-Ti-O(II)$_x$	
	532.37	1.54	18.18	C-Ti-(OH)$_x$	
	533.4	1.21	4.35	Al_2O_3/OR	
	533.8	2.01	12.98	H_2O_{ads}	
$Ti_3C_2T_x$-24h*	529.9	1.14	20.2	C-Ti-O(I)$_x$	3, 50-52
	530.9	0.96	11.5	C-Ti-O(II)$_x$	
	532.2	2.04	58.9	C-Ti-(OH)$_x$	
	533.8	2.13	9.4	H_2O_{ads}	
$Ti_3C_2T_x$-MILD	529.9	1.02	29.9	C-Ti-O(I)$_x$	3, 50-52
	531	1.62	24.9	C-Ti-O(II)$_x$	
	532.1	1.19	34.4	C-Ti-(OH)$_x$	
	533.1	1.9	6.4	Al_2O_3/OR	
	534.1	1.89	5.4	H_2O_{ads}	
$Ti_3C_2T_x$-30h*	529.94	1.06	32.9	C-Ti-O(I)$_x$	3, 50-52
	530.79	1.12	7.46	C-Ti-O(II)$_x$	
	532.08	2.1	50.61	C-Ti-(OH)$_x$	
	533.9	2.13	9.03	H_2O_{ads}	

‡ OR stands for organic compounds/surface contamination.

* Almost no Al was detected for these two samples. Al_2O_3% in these samples is equal to zero.

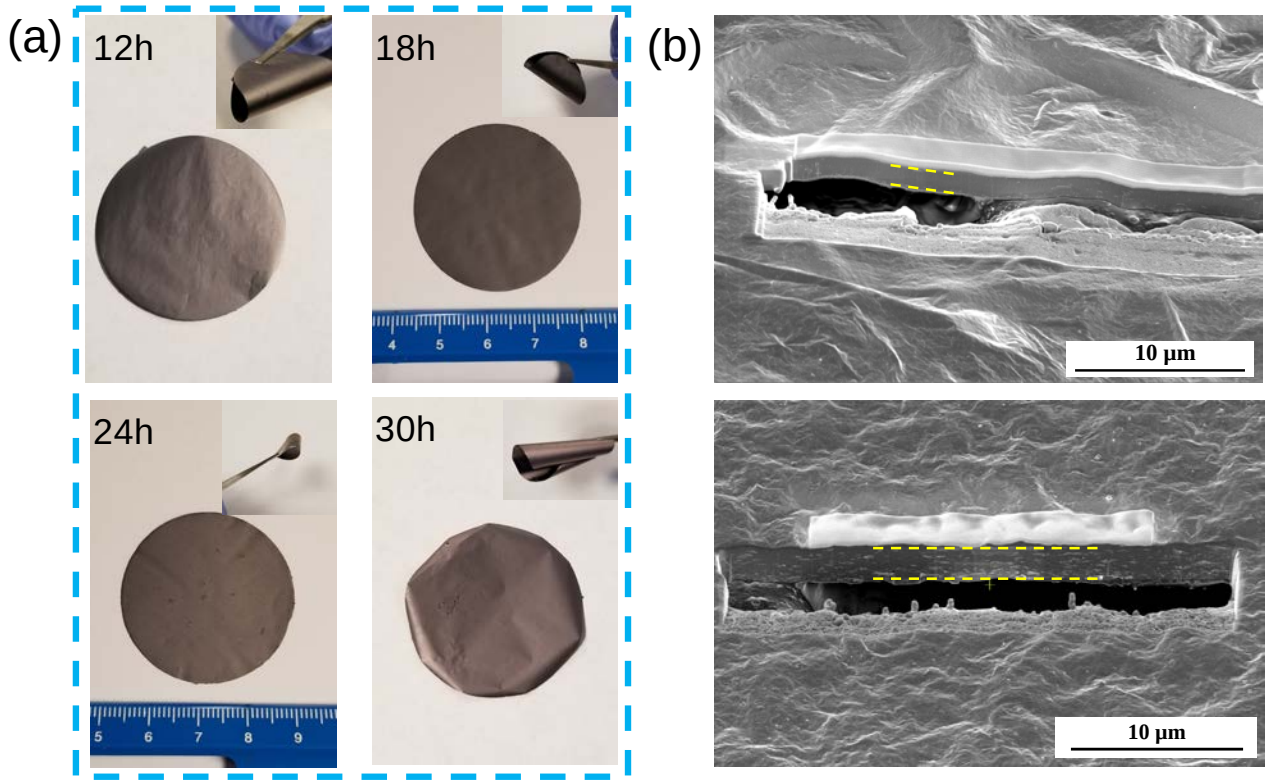

Figure S7. (a) Photographs of free-standing films of EN-MILD 12 h, 18 h, 24 h and 30 h-$Ti_3C_2T_x$ samples fabricated by VAF. The image at the corner of these photographs show the flexibility of the prepared freestanding films; (b) Cross-section of MXene films prepared at two different thicknesses cut with SEM/FIB Dual Beam workstation to measure the thickness of the films. The top MXene film had an average thickness of ≈ 1.4 µm and bottom MXene film had an average thickness of ≈ 2.8 µm. Dash-lines show the cross-section of the films.

Figure S8 shows the CV curve for different synthesized MXene at different rate from1 mv/s to 1000 mv/s. MXene prepared with EN-MILD approach after 24 h etching shows the highest capacitance among the synthesized MXenes.

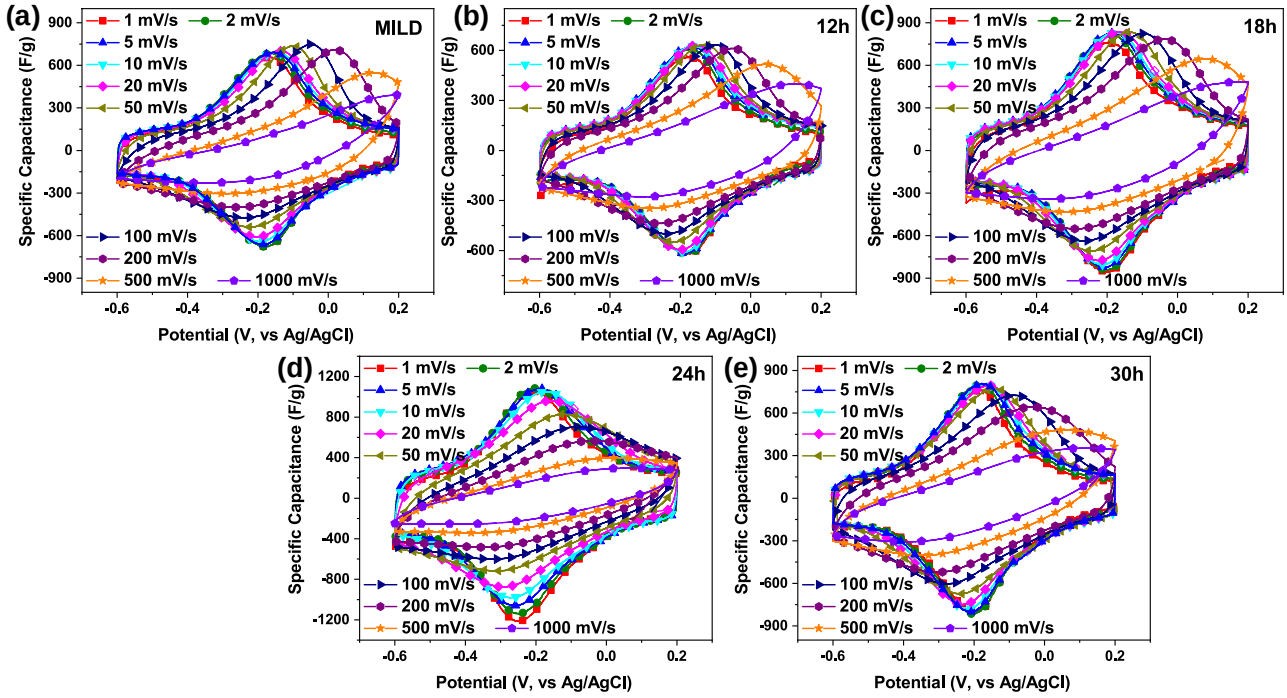

Figure S8. CV curve for different synthesized MXene at different rate, 1 mv/s to 1000 mv/s; (a) MILD, and EN-MILD at different etching times of (b) 12 h, (c) 18 h, (d) 24 h, and (e) 30 h electrodes.

The kinetics of the MXene electrodes prepared by the EN-MILD 24 h etching and traditional MILD approach are analyzed using power law ($i = av^b$), where i is the peak current, a is a constant and v is scan rate, b ranges from 0.5 to 1. A b-value of 0.5 indicates that the current is totally controlled by semi-infinite linear diffusion (diffusion-controlled) while a b-value of 1indicates that the current is surface-controlled (capacitive process). The CV curves recorded at 1 mV s^{-1}, 2 mV s^{-1}, 5 mV s^{-1}, 10 mV s^{-1} and 20 mV s^{-1} are used for the analysis. The results are shown in **Figure S9**.

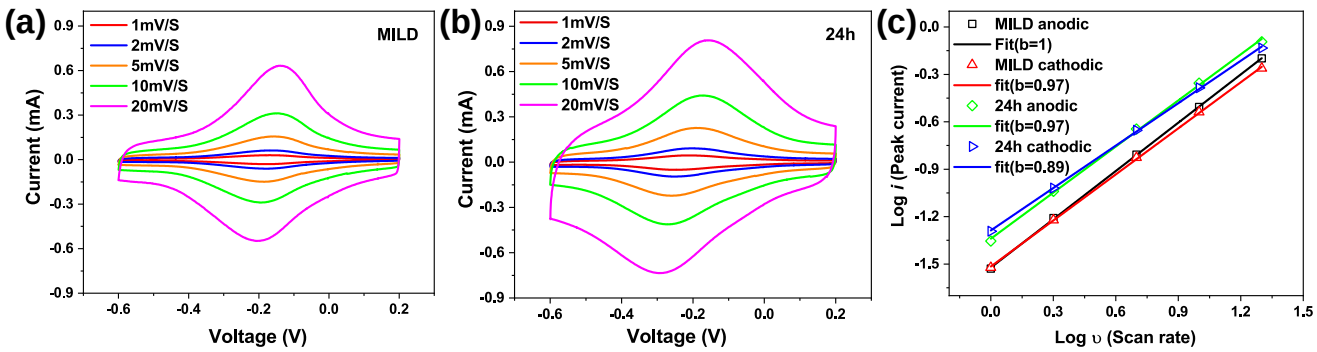

Figure S9. (a) CV curves of the MXene electrode prepared by MILD in 3 M H_2SO_4 electrolyte. (b) CV curves of the MXene electrode prepared by EN-MILD 24h in 3 M H_2SO_4 electrolyte. (c) The relationship between peak current and scan rates from 1 to 20 mV s^{-1} for the MXene electrodes.

Figure S10 indicates the galvanostatic charge-discharge performance of different $Ti_3C_2T_x$ MXene synthesized here at different current densities. MXene synthesized with EN-MILD approach generally demonstrated higher specific capacitance comparing to traditionally MILD approach.

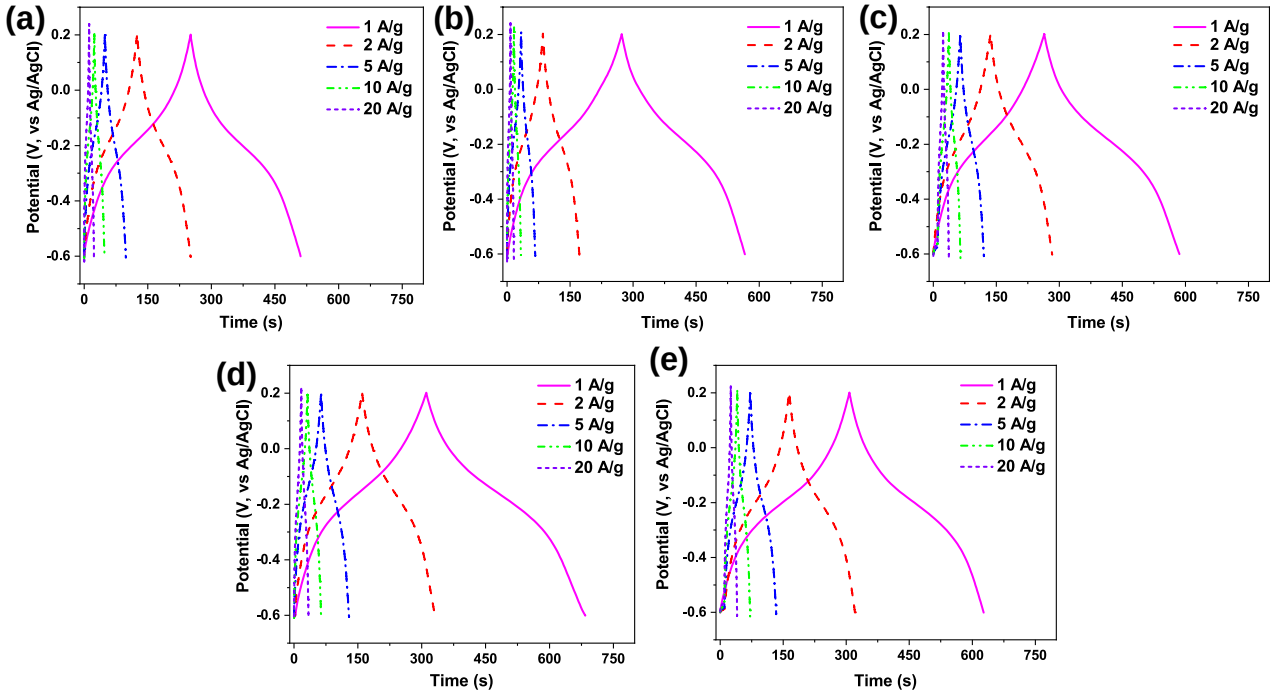

Figure S10. Galvanostatic charge-discharge performance of different $Ti_3C_2T_x$ MXene (a) MILD, and EN-MILD at different etching times of (b) 12 h, (c) 18 h, (d) 24 h, and (e) 30 h electrodes, respectively.

Figure S11 shows the relation between the electrical conductivity and capacitance for different MXene electrodes.

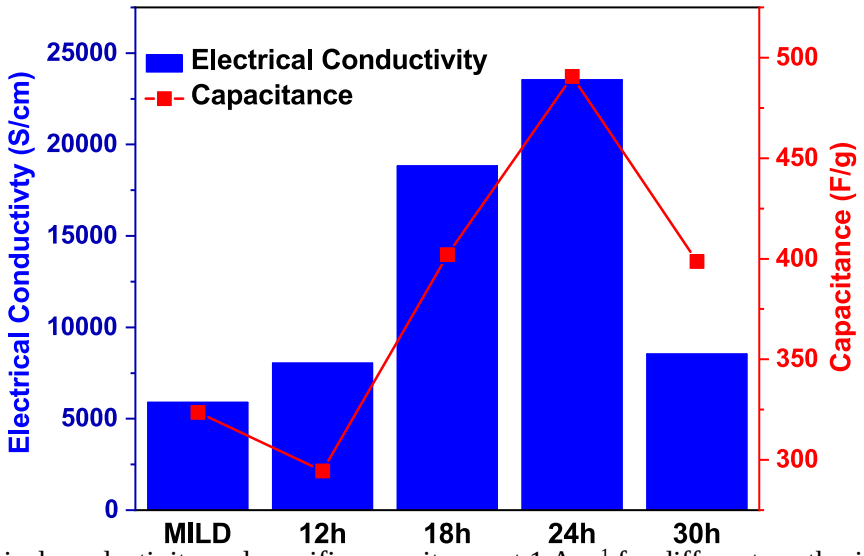

Figure S11. Electrical conductivity and specific capacitance at 1 A g^{-1} for different synthesized MXenes.

References:

1. F. Shahzad, M. Alhabeb, C. B. Hatter, B. Anasori, S. M. Hong, C. M. Koo and Y. Gogotsi, *Science*, 2016, **353**, 1137-1140.
2. M. Alhabeb, K. Maleski, B. Anasori, P. Lelyukh, L. Clark, S. Sin and Y. Gogotsi, *Chem. Mater.*, 2017, **29**, 7633-7644.
3. J. Halim, I. Persson, P. Eklund, P. O. Persson and J. Rosen, *RSC Adv.*, 2018, **8**, 36785-36790.
4. A. D. Dillon, M. J. Ghidiu, A. L. Krick, J. Griggs, S. J. May, Y. Gogotsi, M. W. Barsoum and A. T. Fafarman, *Adv. Funct. Mater.*, 2016, **26**, 4162-4168.
5. M. Ghidiu, M. R. Lukatskaya, M.-Q. Zhao, Y. Gogotsi and M. W. Barsoum, *Nature*, 2014, **516**, 78.
6. E. Kayali, A. VahidMohammadi, J. Orangi and M. Beidaghi, *ACS Appl. Mater. Interfaces*, 2018, **10**, 25949-25954.
7. X. Sang, Y. Xie, M.-W. Lin, M. Alhabeb, K. L. Van Aken, Y. Gogotsi, P. R. Kent, K. Xiao and R. R. Unocic, *ACS Nano*, 2016, **10**, 9193-9200.
8. A. Lipatov, M. Alhabeb, M. R. Lukatskaya, A. Boson, Y. Gogotsi and A. Sinitskii, *Adv. Electron. Mater.*, 2016, **2**, 1600255.
9. H. Huang, H. Su, H. Zhang, L. Xu, X. Chu, C. Hu, H. Liu, N. Chen, F. Liu, W. Deng, B. Gu, H. Zhang and W. Yang, *Adv. Electron. Mater.*, 2018, **4**, 1800179.
10. M. Vural, A. Pena-Francesch, J. Bars-Pomes, H. Jung, H. Gudapati, C. B. Hatter, B. D. Allen, B. Anasori, I. T. Ozbolat and Y. Gogotsi, *Adv. Funct. Mater.*, 2018, 1801972.

11. J. Yan, C. E. Ren, K. Maleski, C. B. Hatter, B. Anasori, P. Urbankowski, A. Sarycheva and Y. Gogotsi, *Adv. Funct. Mater.*, 2017, **27**, 1701264.
12. S. J. Kim, H.-J. Koh, C. E. Ren, O. Kwon, K. Maleski, S.-Y. Cho, B. Anasori, C.-K. Kim, Y.-K. Choi, J. Kim, Y. Gogotsi and H.-T. Jung, *ACS Nano*, 2018, **12**, 986-993.
13. X. Zhang, Y. Liu, S. Dong, J. Yang and X. Liu, *Electrochim. Acta*, 2019, **294**, 233-239.
14. Y. Zhang, M. Qiu, Y. Yu, B. Wen and L. Cheng, *ACS Appl. Mater. Interfaces*, 2017, **9**, 809-818.
15. R. Liu, M. Miao, Y. Li, J. Zhang, S. Cao and X. Feng, *ACS Appl. Mater. Interfaces*, 2018, **10**, 44787-44795.
16. K. Maleski, C. E. Ren, M.-Q. Zhao, B. Anasori and Y. Gogotsi, *ACS Appl. Mater. Interfaces*, 2018, **10**, 24491-24498.
17. J. Liu, H. B. Zhang, R. Sun, Y. Liu, Z. Liu, A. Zhou and Z. Z. Yu, *Adv. Mater.*, 2017, **29**, 1702367.
18. C. E. Shuck, M. Han, K. Maleski, K. Hantanasirisakul, S. J. Kim, J. Choi, W. E. Reil and Y. Gogotsi, *ACS Appl. Nano Mater.*, 2019, **2**, 3368-3376.
19. J. Zhang, N. Kong, S. Uzun, A. Levitt, S. Seyedin, P. A. Lynch, S. Qin, M. Han, W. Yang and J. Liu, *Adv. Mater.*, 2020, 2001093.
20. H. Chen, Y. Wen, Y. Qi, Q. Zhao, L. Qu and C. Li, *Adv. Funct. Mater.*, 2020, **30**, 1906996.
21. L. Shen, X. Zhou, X. Zhang, Y. Zhang, Y. Liu, W. Wang, W. Si and X. Dong, *J. Mater. Chem. A*, 2018, **6**, 23513-23520.
22. X. Dong, Y. Zhang, B. Ding, X. Hao, H. Dou and X. Zhang, *J. Power Sources*, 2018, **390**, 208-214.
23. Z. Ling, C. E. Ren, M.-Q. Zhao, J. Yang, J. M. Giammarco, J. Qiu, M. W. Barsoum and Y. Gogotsi, *Proc. Natl. Acad. Sci.*, 2014, **111**, 16676-16681.
24. J. Guo, Y. Zhao, N. Jiang, A. Liu, L. Gao, Y. Li, H. Wang and T. Ma, *Electrochim. Acta*, 2018, **292**, 168-179.
25. M. Han, C. E. Shuck, R. Rakhmanov, D. Parchment, B. Anasori, C. M. Koo, G. Friedman and Y. Gogotsi, *ACS Nano*, 2020.
26. A. Sarycheva, A. Polemi, Y. Liu, K. Dandekar, B. Anasori and Y. Gogotsi, *Sci. Adv.*, 2018, **4**, eaau0920.
27. H. Wang, Y. Wu, J. Zhang, G. Li, H. Huang, X. Zhang and Q. Jiang, *Mater. Lett.*, 2015, **160**, 537-540.
28. P. Collini, S. Kota, A. D. Dillon, M. W. Barsoum and A. T. Fafarman, *J. Electrochem. Soc.*, 2017, **164**, D573-D580.

29. M. Naguib, O. Mashtalir, J. Carle, V. Presser, J. Lu, L. Hultman, Y. Gogotsi and M. W. Barsoum, *ACS Nano*, 2012, **6**, 1322-1331.
30. G. Ying, A. D. Dillon, A. T. Fafarman and M. W. Barsoum, *Mater. Res. Lett.*, 2017, **5**, 391-398.
31. J. Halim, S. Kota, M. R. Lukatskaya, M. Naguib, M.-Q. Zhao, E. J. Moon, J. Pitock, J. Nanda, S. J. May, Y. Gogotsi and M. W. Barsoum, *Adv. Funct. Mater.*, 2016, **26**, 3118-3127.
32. P. Urbankowski, B. Anasori, K. Hantanasirisakul, L. Yang, L. Zhang, B. Haines, S. J. May, S. J. L. Billinge and Y. Gogotsi, *Nanoscale*, 2017, **9**, 17722-17730.
33. F. Du, H. Tang, L. Pan, T. Zhang, H. Lu, J. Xiong, J. Yang and C. Zhang, *Electrochim. Acta*, 2017, **235**, 690-699.
34. B. Anasori, C. Shi, E. J. Moon, Y. Xie, C. A. Voigt, P. R. C. Kent, S. J. May, S. J. L. Billinge, M. W. Barsoum and Y. Gogotsi, *Nanoscale Horiz.*, 2016, **1**, 227-234.
35. G. Ying, S. Kota, A. D. Dillon, A. T. Fafarman and M. W. Barsoum, *FlatChem*, 2018, **8**, 25-30.
36. H. Kim, B. Anasori, Y. Gogotsi and H. N. Alshareef, *Chem. Mater.*, 2017, **29**, 6472-6479.
37. P. Urbankowski, B. Anasori, K. Hantanasirisakul, L. Yang, L. Zhang, B. Haines, S. J. May, S. J. Billinge and Y. Gogotsi, *Nanoscale*, 2017, **9**, 17722-17730.
38. M. Ghidiu, M. Naguib, C. Shi, O. Mashtalir, L. Pan, B. Zhang, J. Yang, Y. Gogotsi, S. J. Billinge and M. W. Barsoum, *Chem. Commun.*, 2014, **50**, 9517-9520.
39. K. Hantanasirisakul and Y. Gogotsi, *Adv. Mater.*, 2018, **30**, 1804779.
40. L. Verger, V. Natu, M. Ghidiu and M. W. Barsoum, *J. Phys. Chem. C*, 2019, **123**, 20044-20050.
41. B. Akuzum, K. Maleski, B. Anasori, P. Lelyukh, N. J. Alvarez, E. C. Kumbur and Y. Gogotsi, *ACS Nano*, 2018, **12**, 2685-2694.
42. J. Orangi, F. Hamade, V. A. Davis and M. Beidaghi, *ACS Nano*, 2020, **14**, 640-650.
43. J. Liu, Z. Liu, H. B. Zhang, W. Chen, Z. Zhao, Q. W. Wang and Z. Z. Yu, *Adv. Electron. Mater.*, 2020, **6**, 1901094.
44. G. Liu, J. Zou, Q. Tang, X. Yang, Y. Zhang, Q. Zhang, W. Huang, P. Chen, J. Shao and X. Dong, *ACS Appl. Mater. Interfaces*, 2017, **9**, 40077-40086.
45. W. Cao, C. Ma, S. Tan, M. Ma, P. Wan and F. Chen, *Nano-Micro Letters*, 2019, **11**, 72.
46. S. Yang, P. Zhang, F. Wang, A. G. Ricciardulli, M. R. Lohe, P. W. Blom and X. Feng, *Angew. Chem. Int. Ed.*, 2018, **130**, 15717-15721.
47. F. Han, S. Luo, L. Xie, J. Zhu, W. Wei, X. Chen, F. Liu, W. Chen, J. Zhao and L. Dong, *ACS Appl. Mater. Interfaces*, 2019, **11**, 8443-8452.

48. W. Wu, J. Xu, X. Tang, P. Xie, X. Liu, J. Xu, H. Zhou, D. Zhang and T. Fan, *Chem. Mater.*, 2018, **30**, 5932-5940.
49. J. Xuan, Z. Wang, Y. Chen, D. Liang, L. Cheng, X. Yang, Z. Liu, R. Ma, T. Sasaki and F. Geng, *Angew. Chem. Int. Ed.*, 2016, **55**, 14569-14574.
50. I. Persson, L.-Å. Näslund, J. Halim, M. W. Barsoum, V. Darakchieva, J. Palisaitis, J. Rosen and P. O. Å. Persson, *2D Mater.*, 2017, **5**, 015002.
51. M. Benchakar, L. Loupias, C. Garnero, T. Bilyk, C. Morais, C. Canaff, N. Guignard, S. Morisset, H. Pazniak and S. Hurand, *Appl. Surf. Sci.*, 2020, **530**, 147209.
52. T. Schultz, N. C. Frey, K. Hantanasirisakul, S. Park, S. J. May, V. B. Shenoy, Y. Gogotsi and N. Koch, *Chem. Mater.*, 2019, **31**, 6590-6597.
53. M. Ghidiu, J. Halim, S. Kota, D. Bish, Y. Gogotsi and M. W. Barsoum, *Chem. Mater.*, 2016, **28**, 3507-3514.
54. J. Halim, K. M. Cook, M. Naguib, P. Eklund, Y. Gogotsi, J. Rosen and M. W. Barsoum, *Appl. Surf. Sci.*, 2016, **362**, 406-417.
55. F. Sharif, A. S. Zeraati, P. Ganjeh-Anzabi, N. Yasri, M. Perez-Page, S. M. Holmes, U. Sundararaj, M. Trifkovic and E. P. Roberts, *Carbon*, 2020, **157**, 681-692.
56. A. Shayesteh Zeraati, F. Sharif, E. Aliabadian, E. P. Roberts and U. Sundararaj, *ACS Appl. Nano Mater.*, 2020, **3**, 4512-4521.